Stress corrosion cracking of API X-60 pipeline in a soil containing water

B.W. Pan [a,b], X. Peng [a], W.Y. Chu [a,*], Y.J. Su [a], L.J. Qiao [a]

[a] *Department of Material Physics, University of Science and Technology Beijing, Beijing 100083, China*
[b] *Key Lab on Instrumentation Science & Dynamic Measurement of The Ministry Education, North University of China, Taiyuan 030051, China*

Abstract

Stress corrosion cracking (SCC) of a API X-60 pipeline steel in a soil containing 33% water has been investigated using slow strain rate tests and sustained load test of single-edge cracked sample. The results showed that a transgranular SCC in the soil occurred when $\dot{\varepsilon} \leq 3.5 \times 10^{-7}\,\text{s}^{-1}$, and the susceptibility to SCC was about 30%. SCC of the cracked sample in the soil at sustained load could also occur, and the threshold stress intensity factor of SCC was $K_{ISCC} = 0.73K_C$.

© 2006 Elsevier B.V. All rights reserved.

Keywords: API X-60 pipeline; Soil containing water; Stress corrosion cracking; Corrosion-induced stress

1. Introduction

There are two types of stress corrosion cracking (SCC) on the outside surface of the buried pipeline. They are referred to as high pH [1,2] and near-neutral pH SCC [3–13]. High pH SCC generally produces intergranular cracking and occurs only in a relatively narrow cathodic potential range in the presence of a carbonate/bicarbonate environment and at a pH greater than 9 [1,2]. It is generally consider that high pH SCC is controlled by anodic dissolution and the grain boundaries are more susceptibility to dissolution than the grains themselves and so that is where the cracks forms [1,2]. For near-neutral pH SCC with pH 6–8 is generally transgranular [3–15]. Parkins et al. considered that the mechanism of near-neutral pH SCC involved dissolution and the ingress of hydrogen into the steel, however, the evidence in support of hydrogen playing a role in the overall growth process was circumstantial rather than direct [5]. Gonzalez-Rodriguez et al. considered that the mechanism of SCC in API X-80 pipeline steel in 0.01 M NaHCO$_3$ solution was dominated by film rupture and anodic dissolution [13]. Park et al. indicated that transgranular SCC in low-pH bicarbonate solution was developed by a pit-to-stress corrosion crack transition mechanism [14]. Chen et al. considered that hydrogen embrittlement mechanism would become operative following dissolution mechanism for crack initiation and initial growth [15]. Gu et al. indicated that hydro-

gen could diffuse into the specimen around the crack tip during SCC of pipeline steels in the near-neutral pH solution, and hydrogen facilitated the dissolution rate of the steel in the solution, resulting in increasing SCC susceptibility [6].

Most SCC on Canadian pipelines has all been of the near-neutral pH type, and the solution on the surface of the pipeline failed by SCC, which is designated as residual water, has a chemical composition of 101 Ca^{2+}, 75 Mg^{2+}, 76 Na$^+$, 5 Cl$^-$, 1100 HCO$_3^-$, and 15 SO$_4^{2-}$ in mg/l [16]. The aqueous solution with the same composition is called as NS4 solution. Up to now, almost of all experiments of the near neutral pH SCC is carried out in various aqueous solutions simulating the composition of the soil, particularly in the NS4 solution. To simulate the soil, Beavers et al. put a pocket filled with the nature soil into the NS4 solution [12]. The objective of this work is to investigate the possibility of SCC of an API X-60 pipeline in a nature soil containing water.

2. Experimental procedures

The composition of the X60 pipeline steel used in this study was 0.05 C, 0.24 Si, 1.33 Mn, 0.04 Nb, 0.04 V, 0.019 Ti, 0.031 Al, 0.0035 S, 0.014 P, and balance Fe. All specimens were machined from the pipeline with wall thickness of 8 mm. The length and thickness of all specimens were along the length and thickness of the pipeline, respectively. The microstructure is composed of polygon ferrites and a few pearlites, as shown in Fig. 1. The mechanical properties measured by the plate specimens with

* Corresponding author. Fax: +86 10 6233 2345.
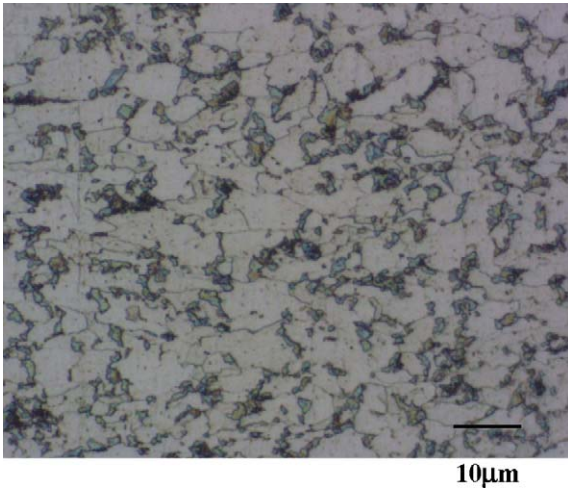*E-mail address:* lqiao@ustb.edu.cn (W.Y. Chu).

Fig. 1. Microstructure of the X60 pipeline steel.

Table 1
Mechanical properties of the API X-60 steel

Thickness (mm)	σ_{ys} (MPa)	UTS (MPa)	Elongation (%)	RA (%)	C_v (J)
5	432	582	30.5	71.2	35
2.5	427	573	19.7	70.9	–
1.5	405	514	15.3	55.3	–
0.5	395	506	13.4	–	–

various thicknesses are listed in Table 1. Table 1 shows that the elongation and the yield strength decreases with decreasing the specimen thickness. The flat tensile specimen with a gage section of 0.5 mm × 2.5 mm is shown in Fig. 2(a). A single-edge notched specimen in dimension of 6 mm × 10 mm × 100 mm containing a notch of 4 mm depth is precracked using three-point bend method to create a fatigue crack of about 1 mm, and then cut into cracked specimens with thickness of 0.5 mm, as shown in Fig. 2(b). The surfaces of the specimens were polished grinding to 800 grit finish using silicon carbide paper, cleared in methanol and air dried.

The soil near a pipeline in Ying county of Shanxi Province of China was used in the study. The ions in the aqueous solution of the soil were analyzed, i.e., 0.984 Ca^{2+}, 0.415 Mg^{2+}, 0.866 Na^+, 0.091 K^+, 0.065 CO_3^{2-}, 0.425 HCO_3^-, 0.262 Cl^-, 0.025 NO_3^-, and 1.825 SO_4^{2-} in ppm. The resistivity and the conduction of the soil were 600 Q/m and 1.8 μ/cm, respectively. The particle size of the soil was about 2–200 μm, and the pore was 35% and the gas was 26%. Stress corrosion cracking was carried out in the soil containing deionized water of 33% in weight, which had a pH value of 8.5, using slow strain rate tests and sustained load test, respectively. Considering low susceptibility to SCC in soil, a lowest strain rate of $7 \times 10^{-8} \, s^{-1}$, at which each sample underwent 1 month, was selected, and in order to study the effect of the strain rate, five strain rates of $\dot{\varepsilon} = 7 \times 10^{-5}, 7 \times 10^{-6}, 7 \times 10^{-7}, 3.5 \times 10^{-7}, 7 \times 10^{-8} \, s^{-1}$ were used. The slow strain rate tests were also carried out in NS4 solution containing 0.122 g $KCl + 0.483$ g $NaHCO_3 + 0.181$ g $CaCl_2 \cdot 2H_2O + 0.131$ g $MgSO_4 \cdot 7H_2O$ per litre of water.

The stress intensity factor of the single-edge cracked specimen is given by [17]

$$K_I = \sigma(\pi a)^{1/2} f\left(\frac{a}{w}\right), \quad f\left(\frac{a}{w}\right) = 1.12 - 0.23\left(\frac{a}{w}\right)$$
$$+ 10.6\left(\frac{a}{w}\right)^2 + 21.7\left(\frac{a}{w}\right)^3 + 30.4\left(\frac{a}{w}\right)^4 \quad (1)$$

where $\sigma = P/BW$ is the applied stress, P is the load, B and W are the width and the thickness of the specimen, and a is the length of the crack. The specimen was loaded in a sustained load machine using weights to fracture and the plane stress fracture toughness, K_C, was obtained through substituting the fracture load into Eq. (1). A set of cracked specimens was loaded in the soil containing water to selected K_I value. When K_I was larger than a threshold stress intensity factor of SCC, K_{ISCC}, the specimen would failure at the sustained load after waiting for a time of t_F. In general, the smaller the K_I, the longer the t_F. K_{ISCC} was obtained based upon the following equation [18]:
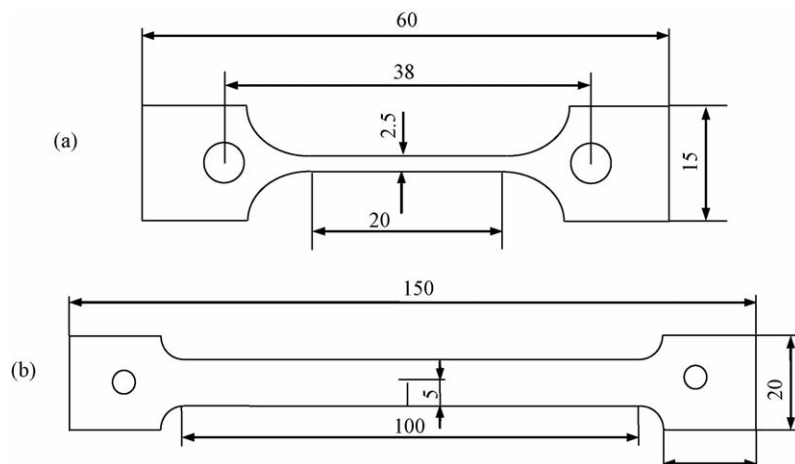
$$K_{ISCC} = \frac{K_{Iy} + K_{In}}{2} \quad (2)$$

Fig. 2. Smooth tensile sample (a) and precracked sample (b) (unit: mm).
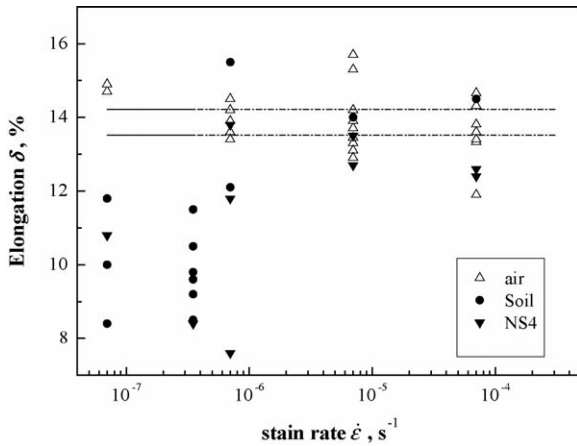
Fig. 3. Elongation straining in air, soil and NS4 solution vs. strain rate.

Fig. 4. Susceptibility to SCC in soil and NS4 solutions vs. strain rate.

$$K_{Iy} - K_{In} \leq 0.1(K_{Iy} + K_{In}) \tag{3}$$

where K_{Iy} was the minimum K_I at which the specimen failure at t_F and K_{In} the maximum K_I at which the specimen would not failure within the fixed time, e.g. 100 h. To ensure the error of measured K_{ISCC} was less than 10%, Eq. (2) must be satisfied, otherwise a new specimen was loaded to $(K_{Iy} + K_{In})/2$. If the new specimen fractured within 100 h, $K_{Iy}^* = (K_{Iy} + K_{In})/2$ and $K_{ISCC} = (K_{Iy}^* + K_{In})/2$. If the new specimen did not fracture, $K_{In}^* = (K_{Iy} + K_{In})/2$ and $K_{ISCC} = (K_{Il}^* + K_{In}^*)/2$.

All tests were carried out at room temperature.

3. Experimental results

3.1. Slow strain rate tests

The variation of the elongation of the samples extending in air, soil containing water and NS4 solution, respectively, with the strain rate $\dot{\varepsilon}$ is shown in Fig. 3. Fig. 3 shows that the average elongation in air is independent upon the strain rate. The mean of 23 samples with various $\dot{\varepsilon}$ is $\delta_0 = 13.87\%$ and the 95% confidence interval of the mean is $\pm 0.36\%$, which corresponds to two doted lines shown in Fig. 3. Fig. 3 shows that when $\dot{\varepsilon} > 7 \times 10^{-7}\,\text{s}^{-1}$, the elongations extending in the solutions is basically consistent with that in air, but decrease evidently when $\dot{\varepsilon} \leq 3.5 \times 10^{-7}\,\text{s}^{-1}$.

The susceptibility to SCC, I_δ, is defined as relative plasticity loss, i.e., $I_\delta\,(\%) = (1 - \delta_{SCC}/\delta_0) \times 100$, where δ_0 and δ_{SCC} are the means of elongations extending in air and in the solutions, respectively. The variation of the susceptibility to SCC in the solutions with $\dot{\varepsilon}$ is shown in Fig. 4. Fig. 4 shows that when $\dot{\varepsilon} > 7 \times 10^{-7}\,\text{s}^{-1}$, no SCC occurs in the soil and NS4 solutions, when $\dot{\varepsilon} \leq 3.5 \times 10^{-7}\,\text{s}^{-1}$, however, SCC occurs and the susceptibility to SCC is about 30%.

The macroscopic fracture of the specimens extending in air reveals cup and cone shape, as show in Fig. 5(a), but that in the soil with $\dot{\varepsilon} \leq 3.5 \times 10^{-7}\,\text{s}^{-1}$ is a plane fracture inclining 45°, as shown in Fig. 5(b) and (c). The macroscopic fracture revealing susceptibility to SCC in the NS4 solution is the same with that in the soil. The fracture surface extending in air is composed of dimple, as shown in Fig. 6(a), and that in the soil with $\dot{\varepsilon} \leq$
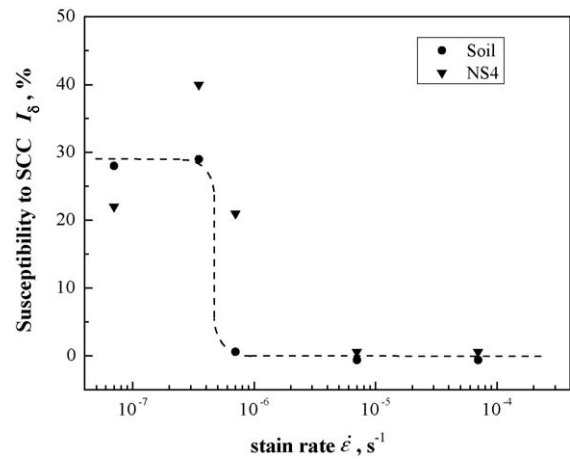
$3.5 \times 10^{-7}\,\text{s}^{-1}$ is composed of quas-cleavage with secondary cracks, as shown in Fig. 6(b) and (c).

3.2. SCC at sustained load

The plane stress fracture toughnesses measured using the single-edge cracked sample were $K_C = 87.6, 90.2, 87.9, 70.7, 76.9\,\text{MPa}\,\text{m}^{1/2}$ with a mean of $K_C = 82.7\,\text{MPa}\,\text{m}^{1/2}$. A set of the cracked sample was loaded in the soil containing water to select values of K_I/K_C. K_I/K_C versus the time to fracture during SCC at sustained load, t_F, is shown in Fig. 7. The hollow points with arrow show no delayed fracture within 100 h. Fig. 7 shows that six specimens generate delayed fracture after keeping the sustained load in the soil for different time, which must due to SCC in the soil solution. Based on Eqs. (1) and (2), we can obtain the threshold stress intensity factor of SCC in the soil solution $K_{ISCC} = 0.73K_C$.

The fracture surface of the cracked sample failured in air was composed of dimple, similar to Fig. 6(a), but that of SCC in the soil at sustained load was composed of quasi-clevage with secondary cracks, similar to Fig. 6(b) or (c).
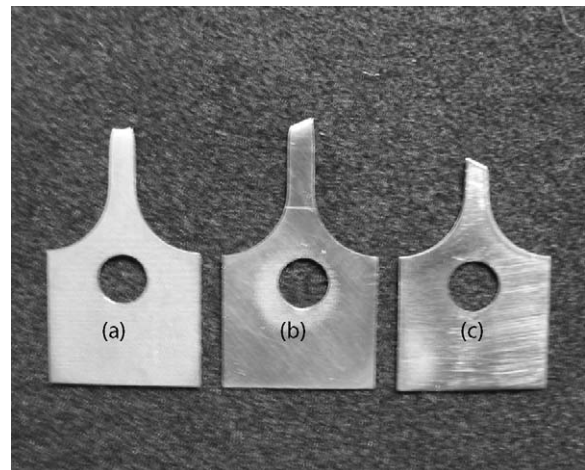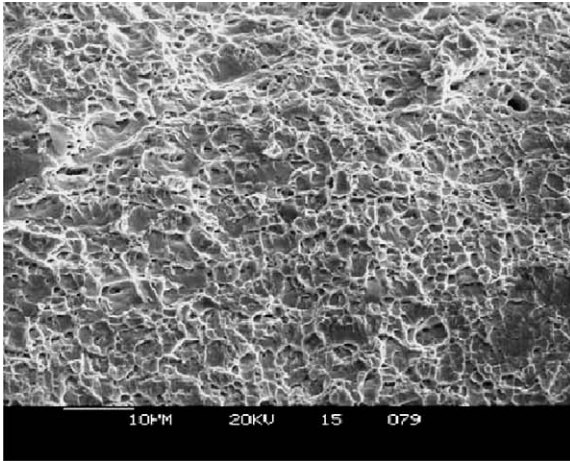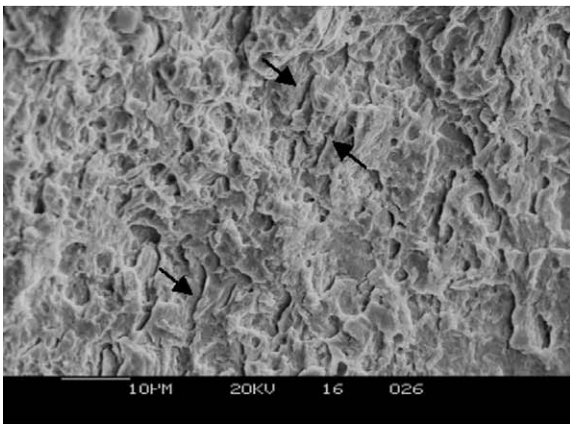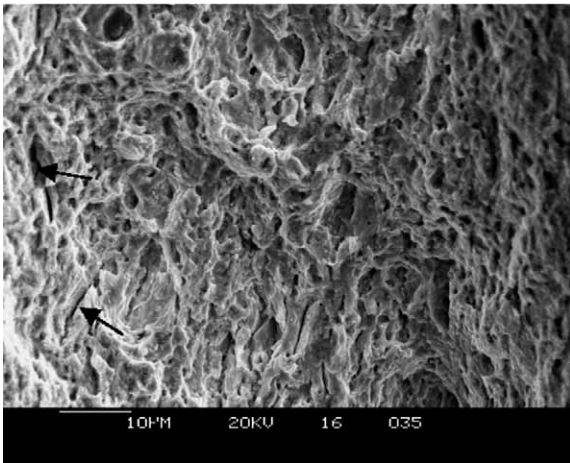

Fig. 5. Macroscopic fractures of the specimens straining in air (a), and in the soil with $\dot{\varepsilon} = 3.5 \times 10^{-7}\,\text{s}^{-1}$ (b) and $\dot{\varepsilon} = 7 \times 10^{-8}\,\text{s}^{-1}$ (c).

(a)

(b)

(c)

Fig. 6. Fracture surfaces of the specimens straining in air (a), and in the soil with $\dot{\varepsilon} = 3.5 \times 10^{-7}$ s^{-1} (b) and $\dot{\varepsilon} = 7 \times 10^{-8}$ s^{-1} (c), respectively. The arrows indicate secondary cracks.

3.3. Stress induced by corrosion in the soil solution

A porous layer appears on surface after corrosion in the soil solution for certain time, as shown in Fig. 8. The flat tensile specimens are extended in air to a plastic strain $\varepsilon_p \geq 1\%$, as shown by curve OA of Fig. 9. After unloading, the specimen is immersed in the soil for 100 h to form a porous layer. After dry-
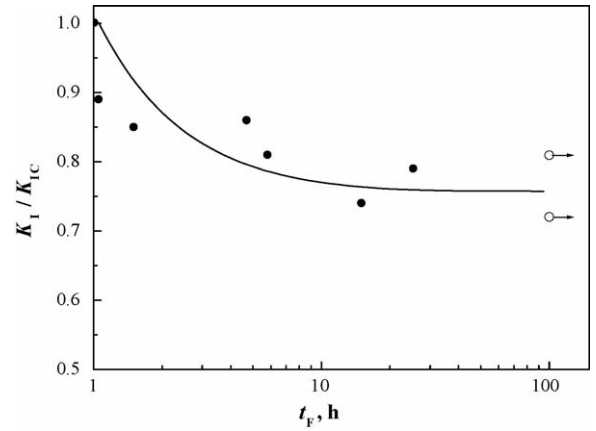

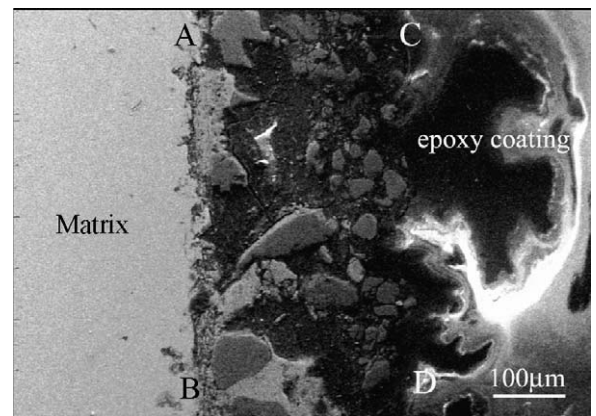Fig. 7. K_I/K_C vs. time to fracture during SCC in the soil at sustained load.

Fig. 8. A porous layer of ABCD after corrosion in the soil for 4800 h.

ing, the corroded specimens are again extended with the same $\dot{\varepsilon}$ in air to over yield, as shown by curve O'B of Fig. 9. The yield stress of the corroded specimen, σ_{ys}^*, which corresponds to the point B in Fig. 9, is less than the flow stress of the specimen before corrosion at unloading point, σ_f, which corresponds to the point A in Fig. 9. Experiments showed that if an unloaded specimen did not corrode, the yield stress during reloading was equal to the flow stress before unloading. Therefore, the dif-
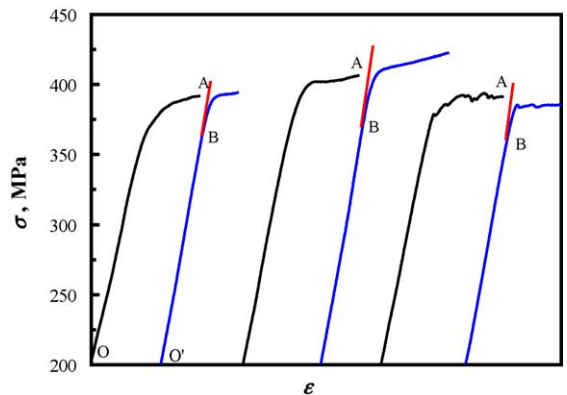

Fig. 9. Stress vs. strain curves extending in air (OA), and that again in air after unloading and corroding in the soil for 100 h (O'B).

ference between σ_f and σ_{ys}^* is defined as the corrosion-induced stress, i.e., $\sigma_p = \sigma_f - \sigma_{ys}^*$ [19–21].

The corrosion-induced stress measured using six specimens were $\sigma_p = 32.5, 33.3, 14.6, 20.4, 12.4$ and 13.8 MPa, respectively. The mean of the additive stress induced during corrosion or SCC in the soil was $\sigma_p = 21$ MPa. Experiment showed that the porous layer after corrosion in the soil for 100 h was about 4 µm, which is 1.5% thickness of the sample. The mean of ultimate tensile strength over 10 specimens without corrosion is 542 MPa, and that over six specimens with corrosion is 538 MPa. Therefore, reduce of the cross-section after corrosion for 100 h is too small to induce the great difference between σ_f and σ_{ys}^*.

4. Discussion

Both slow strain rate tests and sustained load test show that API X-60 pipeline can produce SCC in a soil containing water. For SCC systems controlled by anodic dissolution, e.g. brass in an ammonia solution[19,20], α-Ti in a methanol solution[21] and austenitic stainless steel in a boiling MgCl$_2$ solution [22], there existed a large tensile stress induced by passive film or dealloy layer generated during corrosion or SCC. The corrosion-induced stress could assist the applied stress to enhance localized plastic deformation, resulting in SCC [19–22]. As a result, the potential or pH value dependence of the susceptibility to SCC had a good agreement with that of the corrosion-induced stress [19–22]. The corrosion-induced stress in the porous layer of dealloyed Cu$_3$Au has been calculated through the methods of continuum eigenstrain analysis [23]. The result showed that there was a tensile stress at the porous layer interface decreasing to a maximum compressive stress in the interior of the porous layer, and the maximum tensile stress increased with increasing the thickness of the porous layer [23].

The corrosion-induced stress σ_p can assist the applied stress σ to enhance localized plastic deformation, resulting in SCC. During SCC, the total stress will be $\sigma + \sigma_p$. Substituting the total stress $\sigma + \sigma_p$ into Eq. (1), the stress intensity factor ahead of a loaded crack tip during SCC of the pipeline in the soil will become K_I^*, i.e.

$$K_I^* = (\sigma + \sigma_P)(\pi a)^{1/2} f\left(\frac{a}{w}\right) = K_I + K_{IP} \qquad (4)$$

where σ and K_I are the applied stress and stress intensity factor, respectively, σ_p and K_{IP} are the corrosion-induced stress and corresponding stress intensity factor, respectively. σ_p and than K_{IP} increase with time during SCC because of increase of the thickness of the porous layer. When K_I^* increases to equate the plane stress fracture toughness, K_C, the specimen will failure, and the applied stress intensity factor, K_I, is designated as the threshold stress intensity factor of SCC, K_{ISCC}. Based on Eq. (4), $K_{ISCC} = K_C - K_{IP}$, or

$$\frac{K_{ISCC}}{K_C} = 1 - \frac{K_{IP}}{K_C} = 1 - \frac{\sigma_p}{\sigma_f} \qquad (5)$$

where σ_f is the fracture stress of the cracked sample loaded in air. The mean of five specimens was $\sigma_f = 250$ MPa.

The corrosion-induced stress measured using flowing stress differential method shown in Fig. 9 is an average value over the cross-section of the sample, and the stress measured using deflection method [19,20] is an average value over the thickness of the passive film or porous layer. The latter is two to three times larger than the former [18]. In fact, the maximum corrosion-induced stress should exist near the interface between the porous layer and the matrix [23]. Therefore, the maximum corrosion-induced stress σ_p (max) $= \alpha\sigma_p$ ($\alpha > 1$). Suppose σ_p (max) $= \alpha\sigma_p = 63$ MPa, where $\sigma_p = 21$ MPa is mean measured using flowing stress differential method. Substituting $\sigma_f = 250$ MPa and σ (max) $= 63$ MPa into Eq. (5), we can get $K_{ISCC}/K_C = 0.75$, which is basically consistent with the experiment result of $K_{ISCC}/K_C = 0.73$.

In a word, the corrosion-induced stress increases with time during SCC in the soil containing water, when the total stress, which is the corrosion-induced stress plus an applied stress, is equal to the yield strength, localized plastic deformation occurs under a low applied stress; and when the total stress is equal to the failure stress, delayed fracture occurs during SCC.

Hydrogen entered into sample during SCC in soil will promote SCC. Our recent work indicated that susceptibility to SCC in soil for precharged sample was larger then that for uncharged sample, which was consistence with that precharging increased corrosion-induced additive stress and then increased susceptibility to SCC of brass in ammonia solution [24].

5. Conclusions

1. Transgranular SCC of API X-60 pipeline in a soil containing water can occur at slow strain rate tests with $\dot{\varepsilon} \leq 3.5 \times 10^{-7}$/s, and the susceptibility to SCC is about 30%.
2. SCC in the soil containing water can also occur under sustained load, and the threshold stress intensity factor of SCC is $K_{ISCC} = 0.73K_C$, where K_C is the plane stress fracture toughness.
3. A corrosion-induced tensile stress will generate during corrosion of API X-60 pipeline steel in the soil containing water.

Acknowledgments

References

[1] P.J. Kentish, Br. Corrosion 20 (1985) 139.
[2] J.M. Sutcliffe, R.R. Fessler, W.K. Boyd, R.N. Parkins, Corrosion 28 (1972) 313.
[3] J.A. Beavers, C.E. Jaskece, CORROSION/98, NACE Inter, Houston, TX, 1998, Paper No. 304.
[4] R.N. Parkins, W.K. Blanchards Jr., B.S. Delanty, Corrosion 55 (1999) 312.
[5] R.N. Parkins, CORROSION/2000, NACE Inter, Houston, TX, 2000, Paper No. 363.
[6] B. Gu, J. Luo, X. Mao, Corrosion 55 (1999) 96.
[7] L.J. Qiao, J.L. Luo, X. Mao, Corrosion 54 (1998) 115.

[8] T. Kushidu, K. Nose, H. Asabi, M. Kimura, Y. Yamane, S. Endo, H. Kawano, CORROSION/2001, NACE Inter, Houston, TX, 2001, Paper No. 213.

[9] T.M. Ahmed, S.B. Lanbeot, R. Sutherby, A. Plumtrel, Corrosion 53 (1997) 581.

[10] M.P.H. Brongers, J.A. Beavers, C.E. Jaske, B.S. Delanty, Corrosion 56 (2000) 1050.

[11] T.R. Jack, B. Emo, K. Krist, CORROSION/2000, NACE Inter, Houston, TX, 2000, Paper No. 362.

[12] J.A. Beavers, C.L. Durr, B.S. Delanty, D.M. Owen, R.L. Sutherby, CORROSION/2001, NACE Inter, Houston, TX, 2001, Paper No. 217.

[13] J.G. Gonzalez-Rodriguez, M. Casales, V.M. Salinas-Bravo, J.L. Albarran, L. Martinez, Corrosion 58 (2002) 584.

[14] J.J. Park, S.I. Pyun, K.H. Na, S.M. Lee, Y.T. Kho, Corrosion 58 (2002) 329.

[15] W. Chen, F. King, E. Vokes, Corrosion 58 (2002) 267.

[16] B. Delanty, J. O'Beirne, Oil Gas J. 90 (1992) 39.

[17] W.Y. Chu, J. Yao, C.M. Hsiao, Metall. Trans. A 15 (1984) 729.

[18] G.H. Yu, L.J. Qiao, Y.B. Wang, W.Y. Chu, Corrosion 53 (1997) 762.

[19] X.Z. Guo, K.W. Gao, L.J. Qiao, W.Y. Chu, Metall. Mater. Trans. A 32 (2001) 1309.

[20] X.J. Guo, K.W. Gao, L.J. Qiao, W.Y. Chu, Corrosion Sci. 44 (2002) 2367.

[21] X.Z. Guo, K.W. Gao, W.Y. Chu, L.J. Qiao, Mater. Sci. Eng. A 346 (2003) 1.

[22] J.X. Li, W.Y. Chu, Y.B. Wang, L.J. Qiao, Corrosion Sci. 45 (2003) 1355.

[23] K. Mon, M. Ferrari, Mater. Sci. Eng. A 231 (1999) 88.

[24] K.W. Gao, W.Y. Chu, H.L. Li, Y.P. Liu, L.J. Qiao, Mater Sci. Eng. A 371 (2004) 51.